Eur. Phys. J. D **23**, 143–154 (2003)
DOI: 10.1140/epjd/e2003-00025-9

THE EUROPEAN PHYSICAL JOURNAL D

Electromagnetic resonances of sub-wavelength rectangular metallic gratings

A. Barbara[1,a], P. Quémerais[1], E. Bustarret[1], T. López-Rios[1], and T. Fournier[2]

[1] Laboratoire d'Études des Propriétés Électroniques des Solides, CNRS, 25 avenue des Martyrs, B.P. 166, 38042 Grenoble Cedex 9, France
[2] Centre de Recherche des Très Basses Températures, 25 avenue des Martyrs, B.P. 166, 38042 Grenoble Cedex 9, France

Received 28 May 2002 / Received in final form 26 September 2002
Published online 4 February 2003

Abstract. We present a theoretical and experimental study of electromagnetic modes of 1D sub-wavelength rectangular metallic gratings exposed to P-polarized light. Reflection properties of gratings composed of deep grooves and transmission resonances of gratings composed of deep slits were both examined. Calculations were made using the modal development proposed by Sheng [1]. The aim of this paper is to give a review and detailed description of the theoretical modal method, considering P-polarized light, for both reflecting and transmitting properties. The validity of the method is confirmed by the measured properties of gold-coated microstructured samples. We show that the complementarity between the experiments and the calculations allows to perfectly characterize the EM resonances of the different gratings and to establish a link between the far-field response of these periodic structures and their EM near-field.

PACS. 42.25.Bs Wave propagation, transmission and absorption – 42.25.Gy Edge and boundary effects; reflection and refraction – 42.79.Dj Gratings

1 Introduction

The optical properties of metallic surfaces and particularly the reflectivity of rough surfaces have been intensively studied and are still topics of interest. Until recently these problems were mainly treated in two limiting cases: the case of roughness amplitudes smaller than the wavelength and the case of a very slow profile variation of the roughness on the scale of the wavelength [2]. Moreover, only the physics related to the far-field such as scattering or diffraction of light were investigated. The discovery of the SERS (Surface Enhanced Raman Scattering) in the 70 s has reinforced the interest in rough surfaces as it involved strong and misunderstood phenomena at the surface of the metal, *i.e.* in the near-field. Consequently, many studies devoted to the understanding of the near-field features and their consequences on the far-field properties were undertaken. They focused on the description of complicated electromagnetic (EM) modes of the metal, originating from the photon-surface electron interaction, either considering isolated nanometer objects [3], organized nano-particles [4] or periodic rough surfaces.

Among the large variety of possible rough surfaces, gratings are certainly those which have been the most intensively studied, first of all for their interesting and useful diffractive properties, also for the well-known Wood's anomalies [5] and later in the framework of the comprehension of near-field/far-field response of specific structures exhibiting EM resonances, as was mentioned previously. More recently, a renewal appeared with the technical possibility of realizing (i) periodic gratings on the micrometer or nanometer scale, thus providing samples for simultaneous experimental and theoretical studies, and (ii) roughness amplitudes larger than the wavelength which induce additional EM modes as was theoretically predicted [6] and recently experimentally evidenced [7]. Two fundamental aspects of the EM resonances in gratings emerge from earlier studies. Their occurrence depend on the polarization state of the incident light which can either be P or S. In the following, the P-polarization, also called transverse magnetic (TM), will design the case where the electric field lies in the plane of incidence and the magnetic field is perpendicular to it. The S-polarization, also called transverse electric (TE) will correspond to the case where the electric field is perpendicular to the plane of incidence and the magnetic field parallel to it. The first aspect of the EM resonance concerns the small amplitude grating and corresponds to the Wood's anomalies. These minima in the zero-order reflectivity, occurring for gratings exposed to P-polarized light, correspond to extinctions of the specular reflectivity observed at specific angles. They could not be fully attributed to any diffraction orders, *i.e.* completely explained by a redistribution of the intensity occurring

[a] e-mail: abarbara@grenoble.cnrs.fr

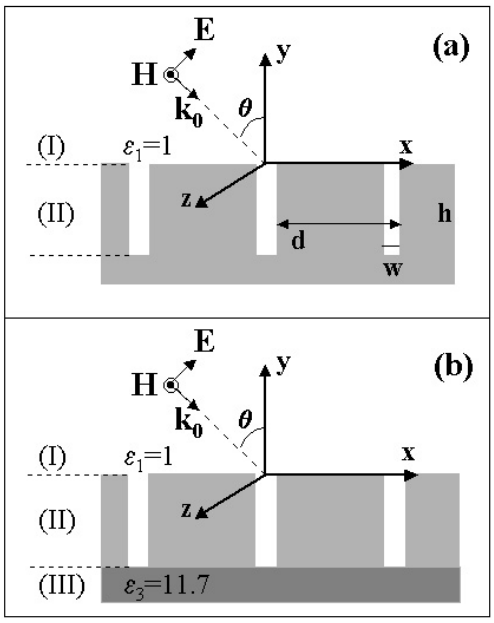

Fig. 1. Schematic representation of the metallic reflecting gratings (a) and transmitting gratings (b) illuminated by P-polarized incident light.

when a new diffraction order emerges from the surface. Several years latter, they were explained by Fano [8] as being actually due to the surface plasmons-polaritons excitation by light. The mechanism by which light induces these surface excitations for weakly corrugated gratings is now well established [9,10]: the corrugation of period d provides to the light a pseudo-momentum $\pm 2\pi n/d$. Under certain circumstances of incidence angle and wavelength, the resulting momentum can be equal to that of the surface charge oscillations. The surface plasmons are excited and propagate along the surface; the reflectivity decreases proportionally to the amount of energy flowing at the interface. The second fundamental aspect of the gratings concerns those with an amplitude larger than or of the order of magnitude of the wavelength. The grooves of width smaller than the wavelength constitute sub-wavelength metallic cavities possessing eigenmodes of frequency depending on the width, the height and the shape of the groove. These resonances, first mentioned by Hessel and Oliner [6], are waveguide-like modes and can arise both in P and S polarization. Properties of parallel metallic strips periodically separated, equivalent to gratings composed of "open" cavities, *i.e.* grooves without any metal at the bottom, through which light can be transmitted, have also been reported [11]. This previous work shows that these types of metallic structure become transparent when the wavenumber tends to zero in P-polarization, *i.e.* when the electric field is perpendicular to the metallic stripes, whereas it becomes semi-transparent in S-polarization.

We have undertaken to produce rectangular metallic gratings composed of sub-wavelength open or closed cavities with large amplitudes, as sketched in Figure 1, and to measure their properties of reflection and transmission for P-polarized incident light. For convenience, the gratings with closed cavities (Fig. 1a) will be called hereafter reflecting gratings, whereas those with open cavities (Fig. 1b) will be named transmitting gratings. Jointly to the measurements, we have carried out calculations based on the exact modal expansion first proposed by Sheng [1] to obtain the far-field response of these devices as well as the EM fields in the whole space and particularly near the grating surface. These calculations have enabled us to understand the physics observed on these devices, in relation with previous theoretical work [8,6,11]. In this paper, we first present in details the theoretical approach we used, considering reflecting and transmitting gratings exposed to P-polarized light. This modal method, used by different groups, was previously well described for reflecting gratings exposed to S-polarized light [12] but was not detailed when used more recently for gratings exposed to P-polarized light [7,13,14]. More generally, the diffraction of metallic gratings was also investigated in the past by other theoretical means [15–18]. However, a detailed review of the calculation and approximations made in P-polarization to obtain the reflection and transmission properties of theses gratings, starting from Sheng's exact method is, as far as we know, missing. This paper has thus the double aim of describing in detail the modal expansion for P-polarized light so that the reader can reproduce the calculations, and to show its reliability and the physics that can be deduced from it, by comparison to the experimental measurement we have jointly performed. After the theoretical description, we present the experimental work *i.e.* the sample elaboration and the far-field detection of the grating's EM modes. The last section will show that both types of gratings exhibit EM resonances which were very well reproduced by the calculations. The resonances, either originating from the surface plasmons polaritons (SPP), the guided type of modes or from a coupling of the two physical phenomena, can be identified by their different dispersion relations and by the spatial near-field distribution at the surface of the grating.

2 Theory

The aim of our work is to investigate the EM resonances of the reflecting and transmitting gratings. To do so, we have determined the expression of the electromagnetic fields as well as the amplitudes of the different reflection and transmission orders. From these we can identify the features of the near-field, *via* the characteristic of the fields at the grating surface, those of the far-field, given by the reflecting and transmitting properties, and the resonances of the system.

The coordinate system of our calculations is represented in Figure 1: the surface is modeled by a perfect rectangular profile of periodicity d composed of grooves of height h and width w. P-polarized light impinges on the gratings with an incidence angle θ. In this geometry the magnetic field **H** is parallel to the z-axis and the electric field **E** lies in the plane of incidence. It is therefore more convenient to calculate the magnetic field, the electric field being easily deduced from Maxwell's equations.

The space is first divided into three regions: the one above the grating of dielectric constant $\varepsilon_1 = 1$, labeled region I, the region of the metallic grating lying in the medium 1, labeled region II and the region beneath the grating of dielectric constant $\varepsilon_3 = 11.7$, labeled region III, and used only when the transmitting gratings are considered. The magnetic field is expressed in each of these regions, and is matched at the boundaries of two regions by applying the continuity conditions of the fields. The study was done either considering a perfectly conducting surface (metal dielectric constant $\varepsilon \approx -\infty$) or a real metallic surface. The assumption of a perfect metallic grating requires that the tangential component of the electric field and the normal component of the magnetic field are nil at the surface of the grating. Considering a grating composed of a real metal implies that the tangential component of the electric and magnetic fields are continuous and different from zero at the surface. To calculate them, we have used the surface impedance approximation [19]. This approach consists in considering a non-zero tangential component of the electric field at the surface of the metal whereas the magnetic field is supposed to have, as for the perfectly conducting surface, only a tangential component, equal to the applied tangential magnetic field $\mathbf{H}_{\mathrm{tg}}^{\mathrm{ext}}$. Solving Maxwell's equations enables to express the tangential component of the electric field at the surface and throughout the skin depth of the metal by

$$\mathbf{E}_{\mathrm{tg}} = Z\left(\mathbf{n} \wedge \mathbf{H}_{\mathrm{tg}}^{\mathrm{ext}}\right) \mathrm{e}^{-(1-\mathrm{i})y/\delta}, \tag{1}$$

where $\mathbf{n}$ is the normal unit vector outgoing from the metal surface into the air, δ is the skin depth of the metal and Z is the surface impedance defined by $Z = \sqrt{\mu_0\mu/\varepsilon_0\varepsilon}$ with μ and ε the relative permitivity and dielectric constant of the metal. We consider here a non magnetic metal with $\mu = 1$.

In the following, only the study concerning real metallic gratings will be presented. However, taking the limit $Z = 0$ in all equations leads to the full results for perfectly conducting gratings.

2.1 Reflecting gratings

In the case where the grooves are closed cavities, we only consider the first two regions I and II, represented in Figure 1a. In region I the magnetic field is expressed by the Rayleigh expansion in plane waves:

$$H_z^{(I)}(x,y) = \mathrm{e}^{\mathrm{i}k_0(\gamma_0 x - \beta_0 y)} + \sum_{n=-\infty}^{+\infty} R_n \mathrm{e}^{\mathrm{i}k_0(\gamma_n x + \beta_n y)}, \tag{2}$$

where $k_0 = \omega/c = 2\pi/\lambda$ is the wavevector and λ the wavelength. The R_n terms are respectively the amplitudes of the n different reflected orders, and γ_n and β_n are given by:

$$\gamma_n = \sin\theta + n\frac{\lambda}{d}$$
$$\beta_n^2 = 1 - \gamma_n^2.$$

In region II, the Rayleigh development is not valid any more as the height of the cavities is far too large in comparison to the incident wavelength. The magnetic field can however be simply expressed using the modal development proposed by Sheng for perfectly conducting [20] or real metal [1] cavities. In the former case, the expression of the field is simple and the matching conditions of the fields at the interface between region I and II lead to a set of linear equations which can be numerically solved to obtain the solution of the problem. For real metallic surface, even though it is more complicated, the field in the region II can also be expressed following Sheng, but the matching conditions lead to a complicated set of non linear equations which can not be easily solved. Due to the difficulty of this procedure, Wirgin *et al.* [18,21] proposed an approximate method which consists in considering the vertical walls of the cavities to be perfectly conducting whereas the horizontal surface at the bottom of the groove obeys the surface impedance condition.

Starting from these assumptions, the expression of the field in region II is determined first considering that it satisfies the Helmholtz equation and can be written as:

$$H_z^{(II)}(x,y) = \left(A\mathrm{e}^{\mathrm{i}k_1 x} + B\mathrm{e}^{-\mathrm{i}k_1 x}\right)\left(C\mathrm{e}^{\mathrm{i}k_2 y} + D\mathrm{e}^{-\mathrm{i}k_2 y}\right),$$

where the wavevectors k_1 and k_2 obey the condition

$$k_1^2 + k_2^2 = k_0^2.$$

The determination of the expressions for k_1 and k_2 and of the relations between the coefficients A and B on one hand and C and D on the other hand, is done using the boundary conditions along the perfectly conducting vertical walls of the cavities:

$$E_y^{(II)} \sim \left(\frac{\partial H_z^{(II)}}{\partial x}\right)_{x=\pm w/2} = 0, \tag{3}$$

and using the surface impedance condition given by equation (1) along the horizontal faces:

$$\left(\frac{\partial H_z^{(II)}}{\partial y} + \mathrm{i}k_0(Z/Z_1)H_z^{(II)}\right)_{y=-h^+} = 0, \tag{4}$$

where $Z_1 = \sqrt{\mu_0\mu_1/\varepsilon_0\varepsilon_1} = \sqrt{\mu_0/\varepsilon_0}$ is the impedance of medium 1.

The solution of these two equations easily leads to the expression for the magnetic field in region II:

$$H_z^{(II)}(x,y) = \sum_{n=0}^{+\infty} A_n \cos\left[\frac{n\pi}{w}\left(x + \frac{w}{2}\right)\right] \mathrm{e}^{\mathrm{i}\mu_n h} \times \left(\mathrm{e}^{\mathrm{i}\mu_n(y+h)} + r_n \mathrm{e}^{-\mathrm{i}\mu_n(y+h)}\right), \tag{5}$$

where A_n is the amplitude of the nth eigenmode of the cavity and $r_n = (Y_n + 1)/(Y_n - 1)$ with $Y_n = (\mu_n/k_0)(Z_1/Z)$ and $\mu_n^2 = k_0^2 - (n\pi/w)^2$. For convenience, we will use the following notation $Z/Z_1 = 1/\sqrt{\varepsilon} = \xi$. Evidently, the limit of the perfectly conducting metal becomes $\xi = 0$.

Using the expression of the fields in regions I and II, the matching conditions are applied at the interface $y = 0$. We know that the boundary condition along a perfectly conducting and non magnetic surface is the continuity of the tangential component of the electric field, whereas the condition above the aperture of the cavities is the continuity of both the tangential components of the electric and magnetic fields. Therefore, the continuity of the tangential component of the electric field is ensured along the whole surface whereas that of the magnetic field is only valid above the apertures of the cavities for a perfect metal. This is expressed as follows:

$$\begin{cases} \left(\frac{\partial H_z^{(I)}}{\partial y}\right)_{y=0^+} = \left(\frac{\partial H_z^{(II)}}{\partial y}\right)_{y=0^-} & x \in [-w/2, +w/2] \\ \left(\frac{\partial H_z^{(I)}}{\partial y}\right)_{y=0^+} = 0 & x \in [-d/2, -w/2] \\ & \text{and} \quad x \in [+w/2, +d/2] \\ H_z^{(I)}(x, 0^+) = H_z^{(II)}(x, 0^-) & x \in [-w/2, +w/2]. \end{cases} \tag{6}$$

Taking into account a real metallic surface *via* the surface impedance condition implies that the tangential electric and magnetic fields obey the relation:

$$\left(\frac{\partial H_z^{(I)}}{\partial y} + \mathrm{i}k_0\xi H_z^{(I)}\right)_{y=0^+} = \left(\frac{\partial H_z^{(II)}}{\partial y} + \mathrm{i}k_0\xi H_z^{(II)}\right)_{y=0^-} = 0 \tag{7}$$

at the surface of the metal, *i.e.* for $x \in [-d/2, -w/2] \cup [+w/2, +d/2]$ and $y = 0$.

The matching conditions, given in (6), are thus replaced, in the case of a good but not perfectly conducting surface, for $x \in [-d/2, +d/2]$ by:

$$\left(\frac{\partial H_z^{(I)}}{\partial y} + \mathrm{i}k_0\xi H_z^{(I)}\right)_{y=0^+} = \left(\frac{\partial H_z^{(II)}}{\partial y} + \mathrm{i}k_0\xi H_z^{(II)}\right)_{y=0^-}, \tag{8}$$

and for $x \in [-w/2, +w/2]$:

$$H_z^{(I)}(x, 0^+) = H_z^{(II)}(x, 0^-). \tag{9}$$

Equation (8) is projected onto the set of basis vectors $\exp(-\mathrm{i}k_0\gamma_m x)$, whereas equation (9) is projected onto the set of basis vectors $\cos\left[\frac{m\pi}{w}(x + w/2)\right]$, periodic over w. The projection onto the $\exp(-\mathrm{i}k_0\gamma_m x)$ is written, noting from equation (7) that the integral in region II is null for $x \in [-d/2, -w/2] \cup [w/2, d/2]$:

$$\frac{1}{d}\int_{-d/2}^{+d/2}\left(\frac{\partial H_z^{(I)}}{\partial y} + \mathrm{i}k_0\xi H_z^{(I)}\right)_{y=0^+} \mathrm{e}^{-\mathrm{i}k_0\gamma_m x}\mathrm{d}x = \frac{1}{d}\int_{-w/2}^{+w/2}\left(\frac{\partial H_z^{(II)}}{\partial y} + \mathrm{i}k_0\xi H_z^{(II)}\right)_{y=0^-} \mathrm{e}^{-\mathrm{i}k_0\gamma_m x}\mathrm{d}x. \tag{10}$$

Inserting the expressions of the magnetic fields and their derivatives in (10) leads to the following expression for the R_m terms:

$$R_m = \left(\frac{\beta_0 - \xi}{\beta_0 + \xi}\right)\delta_{m0} + \frac{\Gamma}{k_0(\beta_m + \xi)} \times \sum_{n=0}^{+\infty} A_n S_{mn}^{-}\left(k_0\xi + \mu_n\right)\left(\mathrm{e}^{2\mathrm{i}\mu_n h} - 1\right), \tag{11}$$

where $\Gamma = w/d$ and the $S_{mn}^{\pm}$ terms are integrals defined by:

$$S_{mn}^{\pm} = \frac{1}{w}\int_{-w/2}^{+w/2}\cos\left[\frac{n\pi}{w}(x + w/2)\right]\mathrm{e}^{\pm\mathrm{i}k_0\gamma_m x}\mathrm{d}x.$$

If $n = 0$ we have $S_{m0}^{+} = S_{m0}^{-} = \mathrm{sinc}(k_0\gamma_m w/2) = s_m$.

The projection onto the set of basis vectors $\cos[\frac{m\pi}{w}(x + w/2)]$ is written:

$$\frac{1}{w}\int_{-w/2}^{+w/2}\cos\left[\frac{m\pi}{w}(x + w/2)\right]H_z^{(I)}(x, 0^+)\mathrm{d}x = \frac{1}{w}\int_{-w/2}^{+w/2}\cos\left[\frac{m\pi}{w}(x + w/2)\right]H_z^{(II)}(x, 0^-)\mathrm{d}x,$$

and after insertion of the fields expression, we obtain:

$$A_m = \left(\frac{2}{1 + \delta_{m0}}\right)\left(\frac{1}{\mathrm{e}^{2\mathrm{i}\mu_m h} + r_m}\right)\sum_{n=-\infty}^{+\infty} S_{nm}^{+}(\delta_{n0} + R_n). \tag{12}$$

Solving this linear equation system (Eqs. (11, 12)) for the amplitudes A_m and R_m allows to numerically calculate these terms and to determine the field in the whole space. The R_m are replaced in (12) by their expression given in (11) to obtain a matrix equation for the amplitudes A_m given by:

$$H\,A = D \quad \text{or} \quad \sum_{\ell=0}^{+\infty} H_{m\ell}A_\ell = D_m$$

with

$$H_{m\ell} = \delta_{m\ell} - \left(\frac{2\Gamma}{1 + \delta_{m0}}\right)(\mu_\ell/k_0 + \xi) \times \sum_{n=-\infty}^{+\infty}\frac{S_{nm}^{+}S_{n\ell}^{-}}{\beta_n + \xi}\left(\frac{\mathrm{e}^{2\mathrm{i}\mu_\ell h} - 1}{\mathrm{e}^{2\mathrm{i}\mu_m h} + r_m}\right)$$

$$D_m = \frac{4\beta_0}{(1 + \delta_{m0})(\beta_0 + \xi)}\frac{S_{0m}^{+}}{(\mathrm{e}^{2\mathrm{i}\mu_m h} + r_m)}. \tag{13}$$

The first step is to truncate the infinite-order matrix to a finite size for the numerical calculations. The values of the $A_0, A_1, \cdots$ terms are then obtained from the inversion of H. Limiting the square matrix (ℓ, m) and the sum over n to finite values L and N amounts to consider the existence of L eigenmodes in the cavities and N reflected orders, which can be propagating or evanescent, L and

N being sufficiently high to have a reliable description of the system. In practice, the solutions are searched for increasing values of (L, N) until a stable solution appears. This stability is rapidly obtained, for typical values $L < 9$ and $N < 50$. Previous works, realized for equivalent gratings exposed to S-polarized light [12,21], mention that even though the solutions can slightly change for $L < 9$, the description of the system in terms of reflectivity values and resonant frequency determination, is very precise when considering only the fundamental eigenmode $\ell = 0$ of the cavity, in the limit of sub-wavelength slit apertures, *i.e.* for $2w < \lambda$. This limit can be understood regarding the wavevectors μ_ℓ of the fields in the cavities given in equation (5). It appears that all the μ_ℓ are imaginary, except when $\ell = 0$, as long as $2w < \lambda$. If w becomes larger than $\lambda/2$, the mode $\ell = 1$ is also propagating and the unimodal approximation is not valid anymore. This unimodal approximation considerably simplifies the equations. Indeed, when considering only the mode $\ell = m = 0$ in equation (2.1) we have:

$$A_0 \left[1 - \Gamma \left(\frac{\mathrm{e}^{2\mathrm{i}\mu_0 h} - 1}{\mathrm{e}^{2\mathrm{i}\mu_0 h} + r_0}\right)(1+\xi) \sum_{n=-N}^{+N} \frac{s_n^2}{\beta_n + \xi}\right] = \frac{2\beta_0}{\beta_0 + \xi} \frac{s_0}{(\mathrm{e}^{2\mathrm{i}\mu_0 h} + r_0)}$$

and

$$R_m = \left(\frac{\beta_0 - \xi}{\beta_0 + \xi}\right)\delta_{m0} + \Gamma A_0 (\mathrm{e}^{2\mathrm{i}\mu_0 h} - 1) s_m \left(\frac{1+\xi}{\beta_m + \xi}\right).$$

Knowledge of the terms A_0 and R_m allows us to calculate the field in the whole space as well as the reflectance properties of the gratings. Resonance frequencies are determined either from the minima in the specular or in the total reflectivity, the latter being classically defined as $R = \sum_{n \epsilon U} \frac{\beta_n}{\beta_0} R_n R_n^*$ where U is the set of n for which the β_n are real. For each frequency resonance, the field near the surface of the gratings can be displayed. This gives an insight into the physical phenomena involved in the resonance as the near-field pattern strongly differs depending on whether surface plasmons or guided modes are excited.

2.2 Transmitting gratings

The transmitting gratings, represented in Figure 1b, are similar to the reflecting gratings except that the grooves are here open cavities. The major aim of calculating the far-field response of these gratings is to determine under which conditions light can be transmitted through these metallic sub-wavelength slits. The theoretical approach is identical to that previously presented for the reflecting gratings, with the difference that region III below the grating has to be taken into account (Fig. 1b). Consequently, additional matching conditions appear, at the interface $y = -h$, between the tangential components of the magnetic and electric fields of the regions II and III. Moreover, the expression of the magnetic field $H_z^{(II)}$ in region II is slightly modified with respect to its expression for reflecting gratings given in equation (5), as it is, in this case, only defined by the condition imposed by the metallic vertical walls. The latter, given by equation (3), leads to the following expression of the magnetic field in region II:

$$H_z^{(II)}(x,y) = \sum_{n=0}^{+\infty} \cos\left[\frac{n\pi}{w}\left(x + \frac{w}{2}\right)\right]\left(A_n \mathrm{e}^{\mathrm{i}\mu_n y} + B_n \mathrm{e}^{-\mathrm{i}\mu_n y}\right).$$

In region I and III, the fields are expressed by the Rayleigh expansion. The expression of $H_z^{(I)}$ remains that given by equation (2) and $H_z^{(III)}$ is described as:

$$H_z^{(III)}(x,y) = \sum_{n=-\infty}^{+\infty} T_n \mathrm{e}^{\mathrm{i}k_0(\gamma_n x - n_3 \beta_{n,t} y)},$$

where T_n is the amplitude of the nth transmitted order, $\beta_{n,t}^2 = 1 - (\gamma_n/n_3)^2$ and $n_3 = \sqrt{\varepsilon_3}$.

The matching condition at the interface $y = 0$ remains the same as for the reflecting gratings (Eq. (8)) and that at the interface $y = -h$ is similarly obtained and expressed by:

$$\left(\frac{\partial H_z^{(II)}}{\partial y} + \mathrm{i}n_3 k_0 \xi_3 H_z^{(II)}\right)_{y=-h^+} = \left(\frac{\partial H_z^{(III)}}{\partial y} + \mathrm{i}n_3 k_0 \xi_3 H_z^{(III)}\right)_{y=-h^-} \quad (15)$$

for $x \in [-d/2, +d/2]$, and

$$H_z^{(II)}(x, -h^+) = H_z^{(III)}(x, -h^-) \quad (16)$$

for $x \in [-w/2, +w/2]$, with $\xi_3 = Z/Z_3 = \sqrt{\varepsilon_3/\varepsilon}$ and $Z_3 = \sqrt{\mu_0/\varepsilon_0\varepsilon_3}$ is the impedance of the medium in region III.

After projection of the matching conditions at both interfaces $y = 0$ and $y = -h$ of equations (8, 15) onto the set of basis vectors $\exp(-\mathrm{i}k_0\gamma_m x)$ and of equations (9, 16) onto the set of basis vectors $\cos[\frac{m\pi}{w}(x + w/2)]$, as was done in the previous subsection for the reflecting gratings, we obtain a set of linear equations between the amplitudes of the modes in the grooves, A_m and B_m, and the amplitudes of the reflected and transmitted orders, R_n and T_n:

$$A_m + B_m = \left(\frac{2}{1+\delta_{m0}}\right) \sum_{n=-\infty}^{+\infty} S_{nm}^{+}(\delta_{n0} + R_n) \quad (17)$$

$$R_m = \left(\frac{\beta_0 - \xi}{\beta_0 + \xi}\right)\delta_{m0} + \frac{\Gamma}{\beta_m + \xi} \times \sum_{n=0}^{+\infty} S_{mn}^{-}\left[A_n(\mu_n/k_0 + \xi) - B_n(\mu_n/k_0 - \xi)\right] \quad (18)$$

$$A_m \mathrm{e}^{-\mathrm{i}\mu_m h} + B_m \mathrm{e}^{+\mathrm{i}\mu_m h} = \left(\frac{2}{1+\delta_{m0}}\right) \sum_{n=-\infty}^{+\infty} S_{nm}^{+} T_n \quad (19)$$

$$T_m = \sqrt{\varepsilon_3}\frac{\Gamma}{\beta_{m,t}+\xi_3}\sum_{n=0}^{+\infty} S_{mn}^{-} \times \left[-A_n \mathrm{e}^{-\mathrm{i}\mu_n h}(\mu_n/k_0-\xi) + B_n \mathrm{e}^{+\mathrm{i}\mu_n h}(\mu_n/k_0+\xi)\right]. \quad (20)$$

Inserting (18) in (17) and (20) in (19) leads to:

$$\sum_{\ell=0}^{+\infty} D_{m\ell}^{I+} A_\ell + \sum_{\ell=0}^{+\infty} D_{m\ell}^{I-} B_\ell = G_m$$
$$\sum_{\ell=0}^{+\infty} D_{m\ell}^{III-} A_\ell + \sum_{\ell=0}^{+\infty} D_{m\ell}^{III+} B_\ell = 0, \quad (21)$$

where

$$D_{m\ell}^{I\pm} = \delta_{m\ell} \mp (\mu_\ell/k_0 \pm \xi)\left(\frac{2}{1+\delta_{m0}}\right)\Gamma \sum_{n=-\infty}^{+\infty} \frac{S_{nm}^{+} S_{n\ell}^{-}}{\beta_n+\xi}$$

$$D_{m\ell}^{III\pm} = \mathrm{e}^{\pm \mathrm{i}\mu_\ell h}\left[\delta_{m\ell} \mp (\mu_\ell/k_0 \pm \xi) \times \left(\frac{2}{1+\delta_{m0}}\right)\sqrt{\varepsilon_3}\Gamma \sum_{n=-\infty}^{+\infty} \frac{S_{nm}^{+} S_{n\ell}^{-}}{\beta_{n,t}+\xi_3}\right]$$

and

$$G_m = \left(\frac{2}{1+\delta_{m0}}\right)\left(\frac{2\beta_0}{\beta_0+\xi}\right) S_{0m}^{+}.$$

The A_m and B_m terms of the **A** and **B** vectors are determined by numerically solving this linear matrix system:

$$D^{I+}A + D^{I-}B = G$$
$$D^{III-}A + D^{III+}B = 0. \quad (22)$$

In the spectral range we have studied these gratings (1.4 to 25 μm), the width of the groove is smaller than the half wavelength. The unimodal approximation can therefore be used as it is sufficient to understand our experimental data and the physics involved, and is much easier to handle. In this approximation, the $D^{I\pm}$ and $D^{IIII\pm}$ terms are no longer matrix but numbers given by:

$$D^{I\pm} = 1 \mp (1 \pm \xi)\Gamma \sum_{n=-\infty}^{+\infty} \frac{s_n^2}{\beta_n+\xi}$$

$$D^{III\pm} = 1 \mp (1 \pm \xi)\sqrt{\varepsilon_3}\Gamma \sum_{n=-\infty}^{+\infty} \frac{s_n^2}{\beta_{n,t}+\xi_3},$$

and the amplitudes of the first mode in the cavity are expressed by:

$$A_0 = \frac{\left(\frac{2\beta_0 s_0}{\beta_0+\xi}\right) D^{III+}}{D^{I+}D^{III+} - D^{I-}D^{III-}}$$

$$B_0 = \frac{\left(\frac{-2\beta_0 s_0}{\beta_0+\xi}\right) D^{III-}}{D^{I+}D^{III+} - D^{I-}D^{III-}}. \quad (23)$$

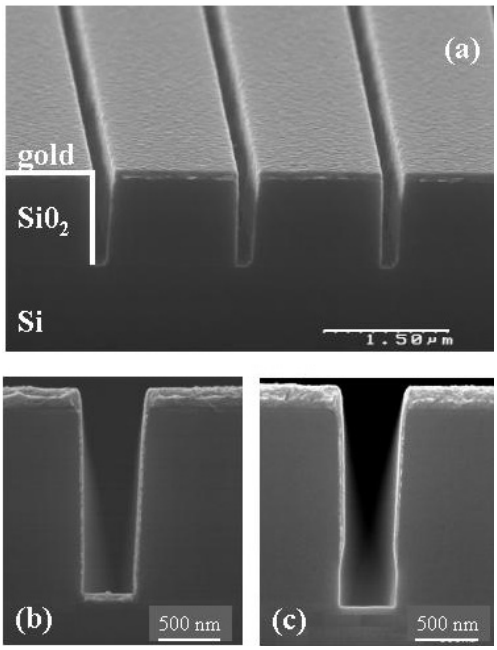

Fig. 2. SEM pictures of the rectangular profile of the surface obtained by periodically etching of silicon oxide on silicon(a) and gold coverage of the whole cavity for the reflecting gratings (b) and of the vertical walls of the cavity for the transmitting gratings (c).

Transmission and reflection properties of these gratings can thus be evaluated. Our results are in very good agreement with those obtained from Lalanne *et al.* who used a semi-analytical one-mode model to calculate the transmission and resonance locations of these types of transmitting gratings, considering a real metal [22].

Moreover, as we will see in the last section, our calculations are also in very good agreement with the experiments and this permits drawing interesting conclusions on the transmission mechanism through such sub-wavelength apertures.

3 Experimental

3.1 Sample preparation

The gratings were fabricated at the LETI-CEA PLATO facility (Grenoble) by standard electron beam lithography. A 1 μm-thick SiO_2 layer was first thermally (TEOS) grown on a {100} silicon wafer. After deposition of an electronegative resist, the sample was irradiated by an electron beam performing horizontal parallel lines of width w, separated by a distance d, over a square area of 6×6 mm^2. The irradiated resist and the SiO_2 beneath were etched away by SF_6 Reactive Ion Etching down to the silicon substrate. After removal of the remaining resist, an almost-perfect rectangular profile of the surface was obtained, as shown in Figure 2a. The resulting structured surface was metallized by thermal evaporation of a gold layer of 60 to 100 nm, much thicker than the skin depth of a few nanometers in

the IR region, in order to prevent transmission of the light through the metal. The adhesion of gold onto the silicon oxide was ensured by an intermediate 30 nm-thick layer of Ti. Two procedures for the metalization were followed, depending on whether reflecting or transmitting gratings were required. In the former case, Ti and Au were successively evaporated at various incidence angles by tilting the sample to obtain a homogeneous coverage over the horizontal surface, as well as over the bottom and vertical walls of the cavities, as shown in Figure 2b. For the transmitting gratings, the bottom of the grooves were preserved from gold coverage by a self-shading effect: the evaporation of Ti and gold was done by tilting successively the sample by an angle $\pm\alpha$ defined by $\alpha \sim \arctan(w/h)$. In this way, light transmission was only allowed through the sub-wavelength cavities formed by the open grooves.

Even though the studied samples are not fully metallic gratings, they are high quality gratings and the approximation to entire metallic structures is excellent. Indeed, the well-controlled procedure of SiO_2 lithography enables to realize an almost-perfect rectangular profile surface (cavity walls less than 10° from the vertical, excellent reproducibility of the period, height and width of the grooves), combined with small dimensions (nominal values of $d = 1.75$ μm, $h = 1$ μm and $w = 0.9$ μm). The validity of the approximation of these samples to fully metallic gratings essentially relies on the quality of the gold coating. For both type of gratings, we found that the gold thickness, even though it is smaller along the walls of the grooves, always remained much larger than the skin depth value. Moreover, the right angles of the rectangular profile, on the top and bottom of the grooves, were fully covered without leaving any uncoated SiO_2 regions.

In the case of the transmitting gratings, we see in Figure 2c, that the gold coverage does not reach exactly the bottom of the vertical walls. However this does not represent a real drawback, the most important being that the two vertical walls are symmetrically covered. Consequently, the height value taken into account for the calculations will be that of the gold layer, and we will keep in mind that the light transmitted by the metallic grating is allowed to go through part of the SiO_2 layer. Finally, we highlight that, in the case of the transmitting gratings, the gold/Si interfaces taken into account for the calculations are in the sample SiO_2/Si interfaces.

3.2 EM modes measurements

The experiments consist in measuring the far-field response of the gratings to an incident P-polarized light. Specular reflectance spectra at various incidence angles and normal incidence transmission measurements were obtained at room temperature, in dry air, in the 1.4 to 25 μm spectral range, with a FTS60A DigiLab Fourier Transform photospectrometer. As the incident beam was not polarized, a linear polarization analyzer was placed in between the outgoing beam (reflected or transmitted) and the detector in order to select the P-polarized response of the grating. The obtained information is equivalent to the one we would have by polarizing the incident beam as, in our geometry where the plane of incidence is perpendicular to the periodicity of the grating, the P and S polarizations are strictly uncoupled and can be treated independently. This would not be true anymore if the incidence plane was not perpendicular to the periodicity of the grating: a fully vectorial theory would then be necessary. The incidence angle was determined with an accuracy of a few degrees only due the divergence of the beam. Finally, for the reflecting gratings, the spectra were all normalized to the reflected intensity of a plane gold layer, evaporated on a non-structured SiO_2, simultaneously to that of the grating. In the case of transmitting gratings, transmission was normalized to that of the 5 mm-diameter hole of the empty sample holder.

4 Results and discussion

The presented experimental results and their comparison to the theoretical work correspond to reflecting and transmitting gratings with the same nominal parameters; $d = 1.75$ μm, $w = 0.9$ μm and $h = 1$ μm. The real parameters, introduced in the calculations, are obtained from scanning electron microscopy pictures. For the reflecting grating we measured $w = 0.7 \pm 0.1$ μm and $h = 1.11 \pm 0.01$ μm and for the transmitting one $w = 0.67 \pm 0.05$ μm and $h = 0.93 \pm 0.1$ μm. The accuracy on the height was much better for the reflecting gratings as it induced by the control of the SiO_2 thickness and etching process and not by the gold coverage along the vertical walls as in transmitting gratings.

4.1 Reflecting gratings

Figure 3 displays the specular reflectivity measured for an incidence angle $\theta = 7.5°$. We notice the existence of several minima which are the far-field signature of the excitation of a resonance of the grating. Indeed, when an EM resonance is excited, part of the EM energy is localized at the surface and/or in the cavities inducing a dip in the reflectivity, proportional to the amount of energy absorbed by the modes. The experimental dips are reproduced in the calculated spectrum. However, we notice that the first dip, appearing at 1 970 cm^{-1}, is much more pronounced in the experimental case than in the theoretical one. This is attributed to the fact that we have considered the vertical walls of the cavities to be perfectly conducting metal. We thus minimize theoretically the quantity of absorbed EM energy and thus the depth of the dip. This phenomenon is less visible on the other peaks as the surface plasmons excitation, which are well described by a realistic dielectric constant, then intervene. As mentioned in the introduction, the EM resonances of the gratings can either originate from the surface plasmons polaritons excitation or from the wave-guide like modes excited in the cavities. In both cases, approximations enable to have a rough feeling of the resonant frequencies. However, to be

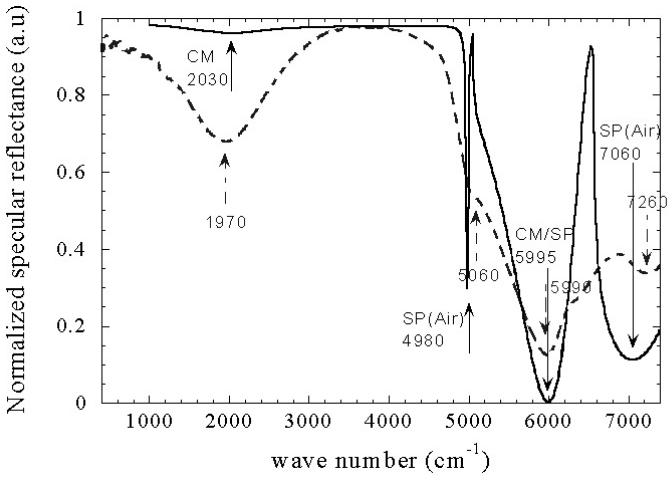

Fig. 3. Specular reflectivity measured on a reflecting grating of parameter $d = 1.75$ μm, $w = 0.7 \pm 0.1$ μm and $h = 1.11 \pm 0.01$ μm, with an incidence angle $\theta = 7.5°$ (dotted line) and theoretical spectra calculated in the multimodal case, considering a real metal, $d = 1.75$ μm, $w = 0.75$ μm and $h = 1.11$ μm (black line). The dielectric function of gold was taken from [23]. Dotted and black arrows respectively indicate the experimental and calculated modes. The CM and SP(Air) symbols take for the cavity modes and the surface plasmons excitations.

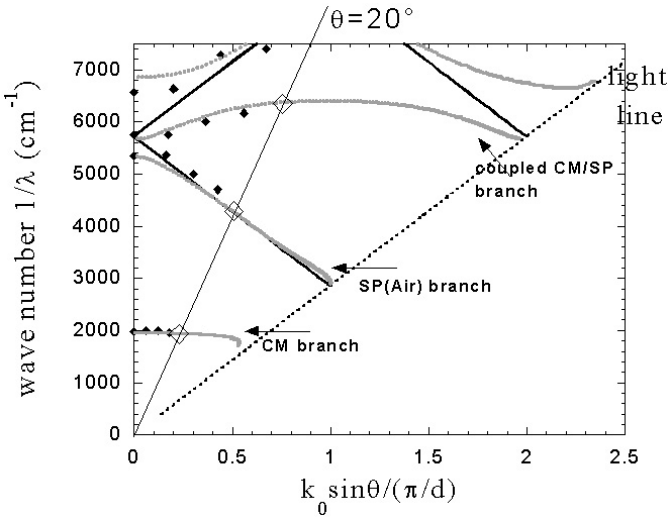

Fig. 4. Theoretical (gray line), experimental (black dots) dispersion relation of the reflecting grating, and surface plasmons (black solid line) dispersion calculated in the approximation of a small roughness periodic surface (Eq. (24)). The dimensions of the gratings are the same as that given in Figure 3. The modes appearing at an incidence angle $\theta = 20°$ are highlighted by open diamonds.

able to undoubtedly attribute each dip to a mode, the full calculation presented in Section 2 has to be undertaken.

As a first approximation, we can consider that the surface plasmon polaritons are excited in the same way as for shallow corrugated gratings:

$$1/\lambda = \frac{n}{d(\sqrt{\varepsilon/(\varepsilon+1)} \pm \sin\theta)}. \quad (24)$$

For a very good metal, as is the case for gold in the infra-red region, this equation basically becomes $1/\lambda = n/d(1 \pm \sin\theta)$ which is strictly equivalent to the condition $\gamma_n = \pm 1$.

In the case of the cavity modes, Lopez-Rios and Wirgin [24] calculated, assuming a sub-wavelength cavity ($w/\lambda \ll 1$), that the resonance should occur, in the case of a perfectly conducting grating, when the relation

$$\coth(k_0 h) = -\sigma \quad (25)$$

is satisfied, where $\sigma = (\Gamma k_0 d/\pi)[\ln(2\pi\Gamma) - 3/2]$. In their approximation, $\Gamma \ll 1$ and $\sigma \to 0$. Consequently, they deduce that the wave-guide modes *approximately* appear at the wavenumbers $1/\lambda = (2n-1)/4h$.

We see from equations (24, 25) that these two types of EM modes can be distinguished by varying the incidence angle θ since the surface plasmons frequencies will be shifted (existence of a dispersion) while those of the guided modes will remain constant (no dispersion). When the height of the grooves is important or when the surface plasmons and guided modes have close resonance frequencies, coupling can occur and these rough approximations are not valid to precisely determine the resonant frequencies; more accurate calculations such as those described in Section 2 have to be undertaken. However, the existence or not of a dispersion as a function of the incidence angle, which appears in these approximations, remains a valid signature. The usual way to find the dispersion relation of an EM mode is to plot its wavenumber $1/\lambda$, proportional to its energy, as a function of its parallel momentum normalized by the length of the first Brillouin zone: $k_\parallel = k_0 \sin\theta/(\pi/d)$, depending on the angle of incidence. The couples $(1/\lambda,\ k_\parallel)$ were obtained from the wavenumbers and the angles of occurrence of the dips in the specular reflectance curves and reported in Figure 4. The experimental points come from curves recorded at $\theta = 0, 5, 7.5$ and $15°$, whereas theoretical points provide from curves calculated at various incidence angles ranging from $0°$ to $20°$. We first remark that the calculated modes describe both the location and the behaviour as a function of the parallel momentum of the measured EM modes. Three different types of modes appear in Figure 4. The first branch, located at $1/\lambda = 1\,960$ cm^{-1}, shows no dispersion and is attributed to the excitation of the first cavity mode ($n = 1$). The second mode occurring at normal incidence at $1/\lambda = 5\,350$ cm^{-1}, follows the black line describing the surface plasmons excitations as given in equation (24) and consequently corresponds to this type of excitation. The behaviour of the third mode, located at $1/\lambda = 5\,680$ cm^{-1} at normal incidence is more complicated. It exhibits no dispersion in the middle of the zone, where no coupling with other modes occur. In contrast, on both extremities of the zone the branch disperses to almost join with the surface plasmon $n = -1$, on the small wavenumber side, and $n = -2$ on the other side. This branch corresponds to the second order wave-guide

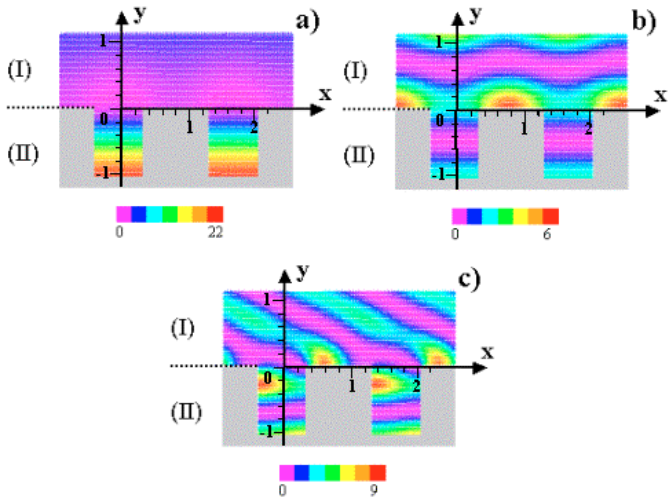

Fig. 5. Magnetic field intensity map at the neighborhood of the grating, calculated for an incidence angle $\theta = 20°$ and taking into account the first ten eigenmodes of the cavity, at the wavenumbers $1/\lambda = 2\,040$ cm^{-1} (a), $1/\lambda = 4\,260$ cm^{-1} (b) and $1/\lambda = 6\,370$ cm^{-1} (c). x and y-axes are displayed in μm and the color scale represents the H-field intensity normalized with respect by the incident field intensity.

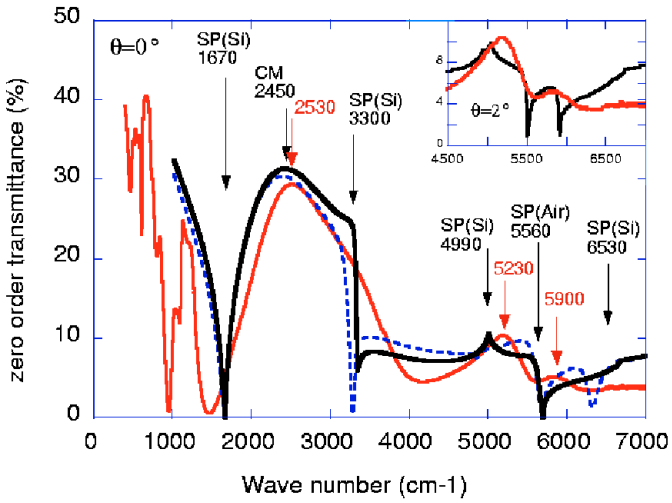

Fig. 6. Experimental normal transmission (red bold line) and calculated spectra within the unimodal approximation (dotted blue line) and in the multimodal case taking four modes within the cavities (black bold line). The black arrows indicate the theoretical excitations of surface plasmon at the air/metal interface with the SP(air) label, of the surface plasmon at the Si/metal interface with the SP(Si) label and the cavity mode with the CM label. Red arrays indicate the experimental regions of enhanced transmission. The inset represents the experimental and calculated spectrum taking a 2° incidence angle into account for the beam divergence.

resonance ($n = 2$), more or less strongly coupled with the surface plasmons modes, depending on the incidence angle.

To get a deeper insight into the physics involved in these resonances, we generated, for various wavenumbers, magnetic field maps in the air near the surface of the grating. This gives a representation of the near-field, when a resonance identified both experimentally and theoretically in the far-field occurs. The differences between the three previously described modes clearly appears. Field maps were calculated for an incidence angle $\theta = 20°$, at the frequencies $1/\lambda = 2\,040$ cm^{-1} (Fig. 5a), $1/\lambda = 4\,260$ cm^{-1} (Fig. 5b) and $1/\lambda = 6\,370$ cm^{-1} (Fig. 5c) corresponding to the resonance frequencies which are highlighted in Figure 4 by open diamonds.

The representation of the magnetic field for the mode at $1/\lambda = 2\,040$ cm^{-1} (Fig. 5a) shows a localization and amplification of the field within the slit, which is in good agreement with a cavity resonance. The surface plasmon excitation modes exhibit quite different features, as can be seen in Figure 5b, as the field is amplified at the surface of the grating. Finally, the coupling which can exist between theses two type of resonances is also clearly illustrated in Figure 5c: a standing wave with two nodes is localized in the groove and coexists with a surface plasmon. For each of these modes, the amplification of the field amplitude is around one order of magnitude. Depending on the incidence angle and on the strength of the coupling between the modes, the amplitude amplification can reach two orders of magnitude, either at the surface of the metal or within the grooves.

4.2 Transmitting gratings

The calculated and measured spectrum of the normal incidence transmission are displayed in Figure 6, for the sample mentioned in Section 3. The experimental zero-order transmission was normalized to the transmission of an empty 6 mm-diameter hole of the sample holder while the calculated zero-order transmission was corrected for multiple incoherent scattering in the silicon substrate. Indeed, the calculated transmission $t = t_0 t_0^* / n_3$ corresponds to the amount of light transmitted by the grating into the silicon substrate. To compare it to the experimental values, we have to take into account the Si/air interface delimiting the sample. We applied to the calculated spectrum the usual correction factor for incoherent multiple scattering within a medium delimited by two flat interfaces (1) and (2) of respective reflection and transmission coefficients t_1, r_1 and t_2, r_2. The total transmission T was thus expressed as:

$$T = \left(\frac{t_0 t_0^*}{n_3}\right) \frac{|t_2|^2}{1 - |r_1|^2 |r_2|^2}.$$

The coefficients r_2 and t_2 at the flat Si/air interface are classically expressed as:

$$r_2 = \frac{n_{\mathrm{Si}} - n_{\mathrm{air}}}{n_{\mathrm{Si}} + n_{\mathrm{air}}}; \quad t_2 = \frac{2n_{\mathrm{Si}}}{n_{\mathrm{Si}} + n_{\mathrm{air}}}.$$

For the interface (1) between the grating and the Si we assumed that $r_1^2 = r_0 r_0^*$, $t_1^2 = t_0 t_0^*$ and $r_1^2 = 1 - t_0 t_0^*$, which

consist in neglecting the absorption. The total transmission reported was consequently finally expressed as:

$$T = \left(\frac{t_0 t_0^*}{3.42}\right) \frac{2.4}{1 - 0.3 \times (1 - t_0 t_0^*)}.$$

This correction was applied to the two calculated spectra reported in Figure 6, respectively, corresponding to the unimodal approximation and to the multimodal case, taking into account four modes within the cavities. Using more modes is not necessary as the numerical convergence was already reached. Both numerical curves are qualitatively identical and, as we will see in the following, the conclusions drawn from the unimodal and multimodal cases on the phenomenon leading to enhanced transmission are the same.

As was reported in the work of Ulrich [11], we find that the calculated and measured transmission is high in the region where $d/\lambda \to 0$, below 1 400 cm^{-1}. In this region, the experimental spectrum also exhibits the SiO_2 and Si phonon absorption which are not reproduced theoretically, as the imaginary part of the Si dielectric constant and the SiO_2 were not taken into account. Above 1 400 cm^{-1}, we clearly see that a highly resonant transmission occurs, for particular frequencies. These transmission properties are analogous to those of 2D metallic holes arrays, reported by Ebbesen *et al.* [25,26]. Previous theoretical works concerning 1D gratings similar to the devices studied in this paper [14,22] proposed two separate mechanisms for resonant transmission: either exciting a cavity resonance able to transmit light through the slits, or transmission due to resonant coupling between plasmons on both interfaces of the grating. These latter modes, also held responsible for the enhanced transmission observed in 2D holes arrays, called "molecular plasmons" modes by Moreno *et al.* [27]. In our experiment, the resonant transmission zones clearly appear at 2 530 cm^{-1} with more than 30% of transmission and at 5 230 and 5 900 cm^{-1} with 12% of transmission. Comparison between the experimental results and our calculations must lead to answering the following questions (i) what are the mechanism involved in the transmission and (ii) are they identical or not to those theoretically proposed [14,22]?

In Figure 6, we see that the calculated spectrum is in good agreement with the experiment, reproducing both the positions and amplitudes of the enhanced transmission zones. However, some differences also appear at frequencies such as 1 670 cm^{-1} or 3 300 cm^{-1} which will be further discussed. Electromagnetic modes due to the surface plasmons, appear at first approximation and as for reflecting gratings, at frequencies for which $\gamma_n = \pm 1$ for the air/metal interface and at frequencies for which $\gamma_n/n_3 = \pm 1$ for the Si/metal interface. Beyond this approximation, we find from equations (23), that the minima in the modulus of $\beta_n + \xi$ and of $\beta_{n,t} + \xi_3$ respectively lead to the surface plasmon excitations at the air/metal and at the Si/metal interfaces. Both are essentially uncoupled owing to the difference in the dielectric constants of Si and air. The surface plasmons at the interface between regions I and II are expected around 5 714 cm^{-1} at normal incidence and at 5 520 and 5 920 cm^{-1} taking an incidence angle of 2° corresponding to the beam divergence (see insert of Fig. 6). These frequencies are very close to those experimentally observed for an enhanced transmission, which gives a first indication on the origin of the surface plasmon excitation at the air/metal interface as a mechanism for enhanced transmission. This result is reinforced by performing H-field maps at the near-field of the gratings. The latter, calculated at normal incidence and for a wavenumber $1/\lambda = 5\,560$ cm^{-1} clearly highlights the nature of surface plasmon through the periodic field-wave localized at the air/metal interface, as shown in Figure 7a. In contrast, the H-field in region III, which signs the transmitted intensity, does not exhibit this feature and $\gamma_n/n_3 \neq \pm 1$. This gives a theoretical indication of transmission enhancement produced by surface plasmon excitations *solely* at the interface air/metal. This indication is confirmed (i) by the experimental observation of this high transmission and (ii) by the fact that no surface plasmons can be experimentally excited at the interface between regions II and III. Indeed, at this interface, the sample does not contain any metal as the Si/metal interface, taken into account in the calculation, is replaced by an Si/SiO_2 interface, the gratings being produced by coating certain segments of the upper side of a SiO_2 surface, as explained in Section 3.1. Etching directly a metallic layer to have a fully metallic grating, identically to the model, would of course be interesting but is a much more challenging process which was not accessible to us. However, it is to note that this disadvantage is also interesting as it enables to completely uncouple experimentally the effect of the surface plasmons appearing at one or the other interface of the grating. Finally, it also explains the strong differences between the experimental and calculated spectra at $1/\lambda = 1\,670, 3\,300, 4\,990$ cm^{-1} corresponding to the condition $\gamma_n/n_3 = \pm 1$, *i.e.* to the Si/metal surface plasmons which are calculated but can not be experimentally observed [28].

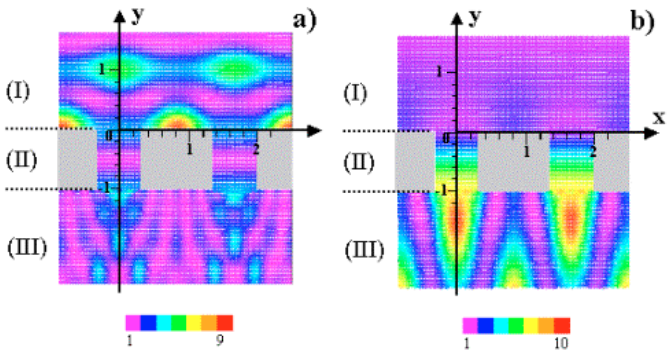

Fig. 7. Magnetic field map intensity at the neighborhood of the grating, calculated for an incidence angle $\theta = 0°$, at the wavenumber $1/\lambda = 5\,560$ cm^{-1} showing the occurrence of transmission in region III due to surface plasmon excitation at the opposite interface between regions I and II (a) and cavity mode at $1/\lambda = 2\,530$ cm^{-1} (b). x and y-axes are displayed in μm and the color scale represents the field intensity normalized to the incidence field intensity.

The cavity mode excitations are obtained when the minima of the denominator modulus in equation (23) is reached. The estimation, to a first approximation, of the location of the resonant frequencies of these cavity modes, was done following the work of Wirgin and Lopez-Rios for the reflecting gratings [24]. We consider an incidence angle $\theta = 0°$ and $w \ll \lambda$ which implies that:

$$s_n = \mathrm{sinc}(k_0\gamma_n w/2) = \mathrm{sinc}(n\pi\Gamma)$$
$$\beta_{n\neq 0} = \mathrm{i}\frac{n\lambda}{d} \qquad \text{and} \qquad \beta_n = \beta_{-n}.$$

Under these circumstances, we have

$$\begin{aligned}\Gamma \sum_{n=-\infty}^{+\infty} \frac{s_n^2}{\beta_n} &= \Gamma - \frac{2\mathrm{i}\Gamma d}{\lambda} \sum_{n=1}^{\infty} \frac{\mathrm{sinc}^2(n\pi\Gamma)}{n} \\ &\simeq \Gamma + \frac{2\mathrm{i}\Gamma d}{\lambda}\left(\ln(2\pi\Gamma) - \frac{3}{2}\right) \\ &\simeq \Gamma + \mathrm{i}\sigma,\end{aligned}$$

where σ is then defined as in equation (25). The latter expression is inserted into the denominator D of the A_0 and B_0 terms given in (Eq. (23)). We then looked for condition satisfying the minima of DD^* corresponding to the cavity resonances, as we stand in a region where no surface plasmon can be excited ($\lambda \gg d$). The minima of DD^* is obtained when

$$\coth(k_0 h) = \left(\frac{1 - \sigma\sigma'}{\sigma + \sigma'}\right), \tag{26}$$

where $\sigma' = \varepsilon_3\sigma$. When σ and $\sigma' \to 0$, *i.e.* when $w \ll \lambda$, this expression tends to the relation $1/\lambda = n/2h$.

Within this approximation, the first cavity mode is expected around $1/\lambda = 2\,750$ cm^{-1}, which is close to the mode measured at $2\,530$ cm^{-1}. Performing the whole calculation enables to find a better agreement with the experiment as the mode is found at $2\,450$ cm^{-1}, as reported in Figure 6. H-field maps calculated for this mode, at normal incidence, confirms the cavity mode excitation as an amplification of the field within the groove characteristic of this mode is observed. It corresponds to the wave guide modes first explained by Hessel and Oliner [6] for deep grooves and proposed by Porto *et al.* [14] for the presented type of structures.

5 Summary and conclusions

In this paper, we have presented a theoretical and experimental study of 1D sub-wavelength rectangular metallic gratings in two cases: reflecting gratings composed of periodically aligned deep grooves and transmitting gratings composed of periodically aligned deep slits. In each case, their far-field properties (reflection and transmission respectively) exhibit specific features associated to the excitation of the EM resonances of these particular systems, when exposed to P-polarized light. We have given here a detailed review of the theoretical approach we used, based of the modal development, which was previously well described in the literature for S-polarized light and reflecting gratings only. In parallel to the calculations, we have fabricated the corresponding samples and measured their reflection and transmission properties at various incidence angles. In the first case, the reflectivity spectrum presents minima corresponding to the excitation of the EM modes which have been identified and characterized. It was shown that the EM resonances linked to the excitation of surface plasmons at the interface between the grating and air localizes EM energy at this interface with a field amplification of one order of magnitude with respect to the incident field. A second type of EM resonance, due to a guided-like mode within the cavities was also identified and tends to localize light in the sub-wavelength regions of the grooves. Finally, a coupling of both type of resonance can appear, leading to a higher amplification of the EM fields. In the case of the transmitting grating, a highly resonant transmission was measured for specific frequencies. We attribute this enhanced transmission to the two different mechanisms also met in the reflecting gratings, namely the cavity modes and the excitation of surface plasmons *solely* at the air/metal interface. The cavity mode was previously well described theoretically in references [14,22]. The excitation of surface plasmons was also discussed but always considering the existence of surface plasmons on both sides of the grating, that would couple through the slits. The occurrence of a softening or a disappearance of the coupling when the dielectric constant between medium I and III become very different was also briefly mentioned to be possible [14]. We have here confirmed experimentally the existence of light transmission through sub-wavelength slits due to cavity modes and shown that the excitation of surface plasmons solely at one side of the grating is also sufficient to enable light transmission. Our interpretation [28] is that, due to the propagating nature of the $n = 0$ mode in the cavities, transmission through these 1D sub-wavelength slits is possible as soon as EM fields can be located at the surface or in the slits, either exciting a cavity mode or a surface plasmon. This makes these devices interesting for applications as very deep cavities can be considered, contrary to the 2D case were the light transmission only occurs by tunneling of the evanescent waves through the holes [27].

We acknowledge the LETI-PLATO facilities for the SiO_2/Si lithography.

References

1. P. Sheng, R.S. Stepleman, P.N. Sanda, Phys. Rev. B **26**, 2907 (1982)
2. F. Toigo, A. Marvin, V. Celli, N.R. Hill, Phys. Rev. B **15**, 5618 (1977), and references therein
3. S.L. McCall, P.M. Platzman, P.A. Wolff, Phys. Lett. **77A**, 381 (1980)
4. F.J. Garcia-Vidal, J.B. Pendry, Phys. Rev. Lett. **77**, 1163 (1996)

5. R.W. Wood, Philos. Mag. **4**, 396 (1902); R.W. Wood, Philos. Mag. **23**, 310 (1912)
6. A. Hessel, A.A. Oliner, Appl. Opt. **4**, 1275 (1965)
7. T. López-Rios, D. Mendoza, F.J. García-Vidal, J. Sánchez-Dehesa, B. Pannetier, Phys. Rev. Lett. **81**, 665 (1998)
8. U. Fano, Ann. Physik **32**, 393 (1938); U. Fano, J. Opt. Soc. Am. **31**, 213 (1941)
9. H. Raether, *Surface Plasmons on smooth and rough surfaces and on gratings* (Springer Tracts in Modern Physics, Springer Verlag, Heidelberg, 1988), Vol. 111
10. V.M. Agranovich, D.L. Mills, *Modern Problemes in Condensed Matter Science; Suface Polaritions* (North Holland, 1982)
11. R. Ulrich, T.J. Bridges, M.A. Pollack, Appl. Opt. **9**, 2511 (1970)
12. A. Wirgin, A.A. Maradudin, Progr. Surf. Sci. **22**(1), 1 (1986), and references therein
13. F.J. García-Vidal, J. Sánchez-Dehesa, A. Dechelette, E. Bustarret, T. Lopez-Rios, T. Fournier, B. Pannetier, J. Light. Techn. **17**, 2191 (1999)
14. J.A. Porto, F.J. Garcia-Vidal, J.B. Pendry, Phys. Rev. Lett. **83**, 2845 (1999)
15. A. Wirgin, R. Deleuil, J. Opt. Soc. Am. **59**, 1348 (1969)
16. D. Maystre, R. Petit, Opt. Commun. **5**, 90 (1972)
17. H. Lochbihler, J. Mod. Opt. **43**, 1867 (1996)
18. A. Wirgin, T. Lopez-Rios, Opt. Commun. **48**, 416 (1984); **49**, 455 (1984)
19. See for example J.D. Jackson, *Classical Electrodynamics*, 3rd edn. (J. Wiley and Sons Inc., 1998)
20. P. Sheng, RCA Rev. **39**, 512 (1978)
21. A. Wirgin, A.A. Maradudin, Phys. Rev. B **31**, 5573 (1985)
22. Ph. Lalanne, J.P. Hugonin, A.S. Astilean, M. Palamaru, K.D. Möller, J. Opt. A: Pure Appl. Opt. **2**, 48 (2000)
23. E.D. Palik, *Handbook of Optical Constants of Solids* (Academic Press, 1998)
24. T. López-Rios, A. Wirgin, Solid State Comm. **52**, 197 (1984)
25. T.W. Ebbesen, H.J. Lezec, H.F. Ghaemi, T. Thio, P.A. Wolff, Nature **391**, 667 (1998)
26. H.F. Ghaemi, T. Thio, D.E. Grupp, T.W. Ebbesen, H.J. Lezec, Phys. Rev. B **58**, 6779 (1998)
27. L. Martín-Moreno, F.J. García-Vidal, H.J. Lezec, K.M. Pellerin, T. Thio, J.B. Pendry, T.W. Ebbesen, Phys. Rev. Lett. **86**, 1114 (2001)
28. A. Barbara, P. Quémerais, E. Bustarret, T. López-Rios, Phys. Rev. B **66**, 161403 (2002)